Paper No.
2521

NACE INTERNATIONAL CORROSION 2013 CONFERENCE & EXPO

AFM Studies of the Adhesion Properties of Surfactant Corrosion Inhibitor Films

Yao Xiong, Bruce Brown, Brian Kinsella, Srdjan Nesic
Institute for Corrosion Multiphase Technology, Ohio University
342 West State Street, Athens, OH 45701, USA

Alain Pailleret
Laboratoire Interfaces et Systèmes Electrochimiques, CNRS, UPR 15
4, Place Jussieu, F-75005, Paris, France

ABSTRACT

The properties of an adsorbed corrosion inhibitor – Tall Oil Fatty Acid (TOFA) imidazolium chloride, on mica, gold and X65 steel were studied using *in-situ* atomic force microscopy (AFM). Topography images and thickness measurements show that the structure of inhibitor film changes from monolayer to bi-layer as inhibitor concentration exceeds its Critical Micelle Concentration (CMC). Further kinetic study indicates that the developing of a full film takes about 6 hours. Quantitative force measurements were performed to evaluate the mechanical and adhesion properties of inhibitor films. Results show that the stress, needed to physically remove adsorbed inhibitor molecules is of the order of MPa.

Key words: corrosion inhibitor, film thickness, adhesion, mechanical resistance, *in-situ* AFM.

INTRODUCTION

Surfactant corrosion inhibitors can retard acidic corrosion when added to the aqueous environment in very small concentrations (ppm level). Nitrogen-based organic molecules, such as imidazolines, imidazoline amido amines and their salts, have been widely used as corrosion inhibitors for protecting mild steel from CO_2 corrosion.[1-4] One of the most important properties of surfactant-type corrosion inhibitors is their ability to adsorb onto a metal surface to form a protective layer.[5-7] Understanding the adsorption mechanism and adhesion strength of these layers is one critical step leading to better understanding of how they perform their corrosion protection function. It is also an important factor when evaluating and selecting an inhibitor for a field application, and when developing models of corrosion in the presence of inhibitors.

Over the last few decades, the adsorption characteristics of a wide variety of surfactants have been investigated, using calorimetry,[8-9] fluorescence decay,[10-11] neutron reflection,[12-13] and atomic force microscopy.[14-18] One important property of a surfactant is its critical micelle concentration (CMC) which is the concentration when the surfactant molecules spontaneously agglomerate together to form small

colloid particles called micelles within the bulk liquid. The micelles significantly affect the adsorption structure of surfactant inhibitors at solid/liquid interfaces and their performance.[19-20] A previous study of surfactant adsorption reported that the formation of a first adsorbed layer was due to electrostatic interactions of positive ions on negatively charged surfaces. The second layer is formed with a further increase in surfactant concentration close to the CMC. In this "bi-layer" arrangement, the hydrocarbon "tails" of the inhibitor molecules are facing each other (inwards) while the hydrophilic groups point outwards – toward the solution and the steel surface.[6,11,21-22] Other adsorption structures are found above the CMC, such as micelles, hemimicelles and admicelles, and have also been reported for various surfactants.[23-25] It has been found that the adsorption and aggregation structures of corrosion inhibitors may vary due to changes in the type of molecules, pH, temperature, counterions and surface properties of the substrate.[26-30]

Nevertheless, some adsorption properties of corrosion inhibitors, such as film thickness, mechanical resistance and adhesion strength, have not been satisfactorily resolved. Studying these properties is very important for understanding the stability and integrity of adsorbed inhibitor films in corrosive environments. A main driver for this work is the widespread discussion that inhibitor film can be removed from the metal surface at some critical fluid velocity.[31-34] This velocity apparently depends on the concentration and type of corrosion inhibitor and is manifested by a rapid increase in the corrosion rate when inhibitor molecules are removed from the surface. Schmitt reported that the performance of inhibitor films decreased when the flow velocity exceeded a critical value, indicating that high shear stress can cause the removal of inhibitor film and inhibition failure. Amongst many others, Zheng *et al* also claimed that high shear stress flow can remove inhibitor layers and significantly decrease their efficiency[33]. However, other well controlled studies have shown that the film integrity was not affected by a high wall shear stress and intense near-wall turbulence.[35] Therefore the resolution of these contradicting findings could only be found by directly measuring the magnitude of the adhesion forces between the steel surface and the inhibitor film and comparing it to the typical hydrodynamic forces seen in the field.

Since the invention of atomic force microscopy (AFM) in 1986,[36] great advances have been made in the application of this technique. AFM has the advantage and capability of being able to measure the forces of molecular interaction and adsorption at surfaces. In this work, an *in-situ* AFM was applied to resolve the structure of adsorbed inhibitor film, to evaluate the mechanical properties of the film, and to determine the stress values needed to remove the inhibitor molecules from the surface. Results show that the stress required to physically remove an inhibitor film is of the order of MPa, which is at least three orders of magnitude higher than the typical wall shear stress seen in turbulent pipe flow. This indicates that protective inhibitor films could not be removed from internal pipe walls by the mechanical forces of the fluid flow alone.

EXPERIMENTAL PROCEDURE

Materials

The molecular structure of corrosion inhibitor Tall Oil Fatty Acid (TOFA) imidazolium chloride is shown in Figure 1. As a 2 nm long cationic surfactant inhibitor, it has a positively charged hydrophilic head and a hydrophobic tail. These molecules can adsorb onto a metal surface and markedly change the corrosion-resistance properties of the metal.[37-39]

The critical micelle concentration (CMC) of TOFA imidazolium chloride (Figure 2) was obtained by measuring changes in surface tension with concentration using the drop weight method.[40] All solutions were prepared using deionized water with a conductivity of 18 MΩ cm^{-1}. The CMC was determined to be 8 mM at pH 4.8 and 25°C.

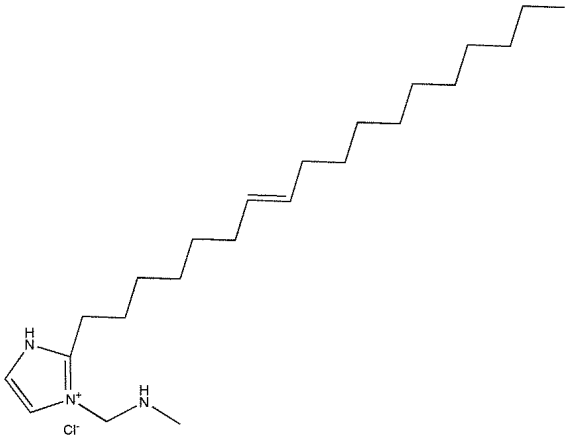

Figure 2: Molecular structure of TOFA imidazolium chloride.

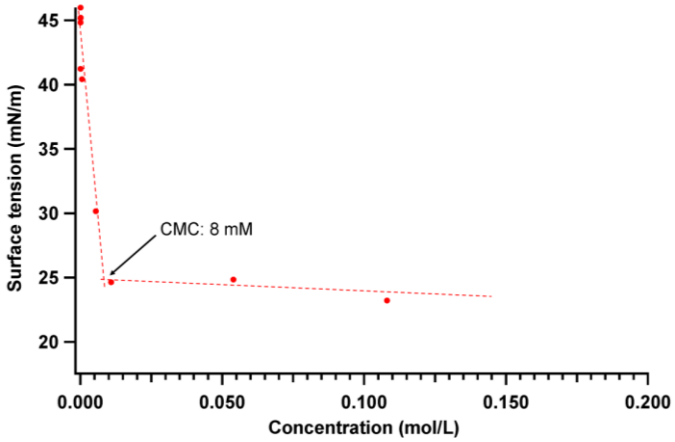

Figure 1: The critical micelle concentration (CMC) for TOFA imidazolium chloride is 8 mM.

Mica was first used to develop the AFM techniques for measuring adsorbed film thickness, normal force and lateral force measurements, because it can provide atomically flat, chemically stable and negatively charged surface for inhibitor adsorption making AFM scanning relatively easy to do and interpret. Subsequent measurements were made on the surfaces of gold and mild steel. The gold surface was prepared by vapor deposition of gold, under high vacuum, onto a polished 316 stainless steel substrate. The steel specimen was cut from a sample of X65 grade mild steel pipe, successively polished using 400, 600, 800, 1000 and 1500 grit silicon carbide paper followed by 9, 3 and 1 μm diamond suspensions. For analysis carried out on the steel surface, both the AFM chamber and the inhibitor solution were deoxygenated using CO_2 in order to eliminate the interference by oxygen corrosion.

Instrument

Figure 3a shows the basic principle of an AFM. The interaction between a scanning probe and the sample surface is measured by means of the cantilever deflection and with the help of an optical laser-based detection system. The AFM probe consists of a force sensor, i.e. a sharp tip mounted on a flexible cantilever, and the tip is usually several microns long and less than 50 nm across (Figure 3b). In *contact* AFM mode, the tip gently "touches" the surface, and the sensed interaction forces between the tip and the surface molecules lead to a small deflection of the cantilever that can be converted into a force using Hooke's law. The cantilever deformation is monitored by a laser reflected from the beam onto a four quadrant photo-sensitive diode detector. These measurements are converted into topographic images, and used to determine the perpendicular and lateral bending of the cantilever. The perpendicular and lateral bending/force measurements can be used generate force-distance curves and friction loops respectively. The force-distance curves records the AFM tip-sample surface interaction as a function of tip-sample distance when the tip is moved perpendicularly to the surface. The friction loops are generated from a line scan in which the tip is moved in a line back and forth (trace and re-trace) across the sample surface. The tip-sample interaction in lateral direction is recorded in the friction loops.

For AFM measurements, the aqueous solution of corrosion inhibitor was prepared at concentrations of 0.5 and 2 times the CMC (i.e. 4 and 16 mM respectively). A freshly cleaved mica, vapor deposited gold, or polished steel substrate, was immobilized in a fluid cell (Figure 4), and the cell was assembled in the AFM instrument with the AFM tip positioned above the substrate surface. Aqueous solution was slowly injected into the cell through the side-tubing. Inhibitor film was allowed to fully develop on the surface for a period exceeding 6 hours, an optimized duration justified later in this paper. AFM measurements were then carried out in aqueous solutions at the solid-liquid interface to obtain surface morphology,

film thickness, penetration and lateral force measurements. The scan rate for imaging and lateral force measurements was set to 1000 $nm.s^{-1}$.

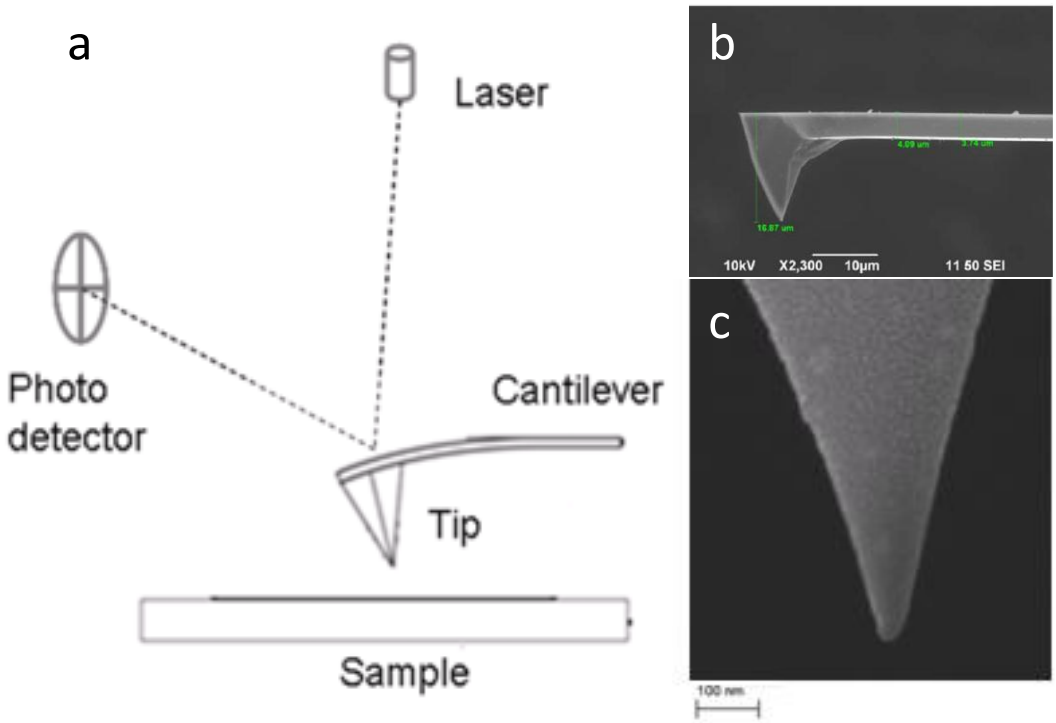

Figure 3: (a) Schematic diagram of the basic principle of AFM; (b) SEM image of a typical AFM tip; (c) the apex portion of the AFM tip used in the present study, where the diameter was measured to be approximately 30 nm.

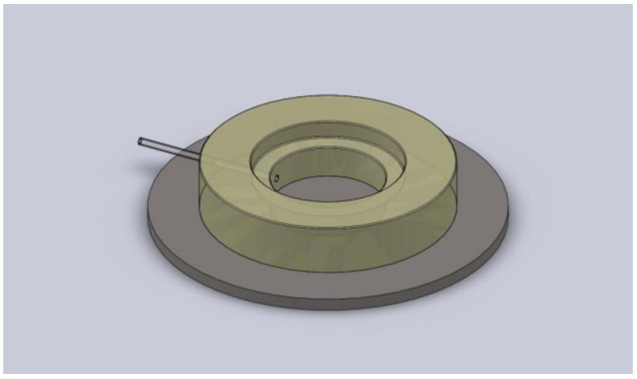

Figure 4: Schematic drawing of the fluid cell used in AFM experiments. The substrate was immobilized in the center of this cell and aqueous inhibitor solution was injected through the side tubing.

The AFM tips is made of Si_3N_4 and mounted on triangular cantilevers with an average spring constant of 0.4 N m^{-1}. They are known to have a rather hydrophobic character and their low spring constant was chosen to help maintaining the integrity of the inhibitor film during scanning in aqueous solutions. To image the topography of the adsorbed molecular structure, a low normal force (< 2 nN) was applied to the AFM cantilever which provides a necessary load for imaging and still avoids damaging the delicate inhibitor film structure.

The method to measure film thickness was to first scratch away a small section of the inhibitor film by lateral sweeps (all the way to the original substrate surface) and then image and measure the height

difference between the scratched and untouched areas. To investigate the forces required for scratching away of adsorbed inhibitor molecules, the normal force applied to the cantilever was gradually increased until lateral cantilever movement was able to damage and remove inhibitor molecules from the substrate surface. The minimal normal force to achieve the removal of adsorbed inhibitor molecules from the various substrate surfaces was determined to be 60 nN. In the first step of this procedure, an XY lateral scan was performed on an area of 1 x 1 μm^2 while still maintaining a high normal force of ≥60 nN. In the second step, a portion of the surface slightly larger than the scratched area was imaged using again a low normal force (< 2 nN) to characterize the damage created by the first step. In addition, a line scan, using this low normal force, traversing the unscratched, scratched and unscratched areas was used to determine film thickness in a slightly different way.

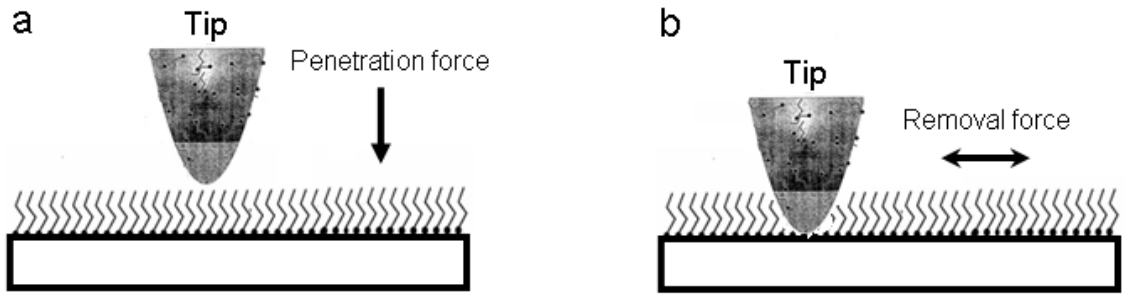

Figure 5: Schematic diagrams of (a) the penetration force measurement and (b) the lateral removal force measurement.

The penetration forces determined in this study were obtained using force-distance curve measurements. They were carried out in-situ within the inhibited aqueous solution and consist of recording the tip-sample interaction as a function of tip-sample distance when the tip is moved perpendicularly to the surface (Figure 5a). Measurements of the lateral force to scratch away inhibitor molecules from substrate surfaces were made using the in-situ friction loop technique. This involved a forward and reverse line scan parallel to the surface and perpendicular to the long axis of the AFM cantilever, under an optimized normal load (Figure 5b). The optimized normal load was 60 nN and was the same as that used for the film thickness measurements. Using the same normal force in each friction loop allows direct comparison between measurements.

RESULTS

Measurements on Mica

Adsorption Structure and Film Thickness

Figure 6 (a) and (b) show surface morphologies of thin films adsorbed on mica from an aqueous TOFA imidazolium chloride solutions containing 0.5 and 2 times the CMC respectively. The topography images were obtained over an area of 1 x 1 μm^2. The surface profile plots show that the surface "roughness" in both conditions is less than 1 nm. The uniform featureless surfaces shown in these images indicate the inhibitor molecules are adsorbed at the mica/solution interface as a continuous (pinhole free) film, flat at the atomic scale. This is regardless of the internal structure of the film which could vary. No artifacts are shown in the images indicating that the adsorbed structure was not disrupted by the scanning process. Multiple images on different locations of the surface confirmed that the mica/solution interface was fully covered by a flat inhibitor film at concentrations of both 0.5 and 2 times the CMC.

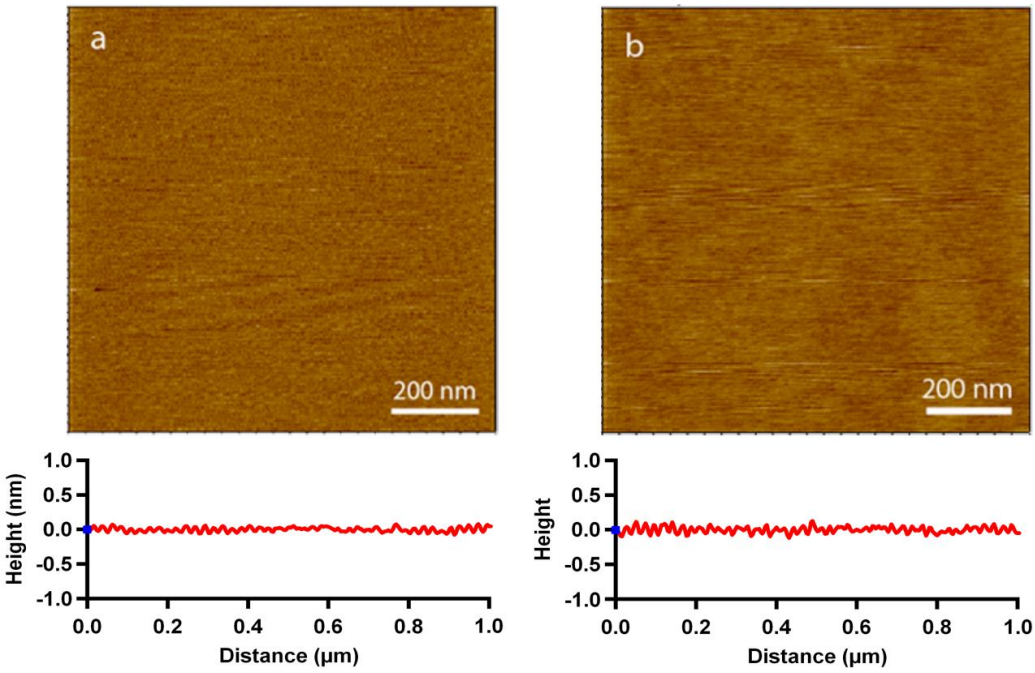

Figure 6: Topography images and surface profiles of inhibitor films formed on mica at (a) 0.5 CMC and (b) 2 CMC. The surface roughnesses at both conditions are less than 1 nm.

To investigate the internal structure of the inhibitor films and to accurately measure film thickness, the inhibitor molecules were removed by scratching the surface over an area of 1 x 1 μm^2. Figure 7 shows AFM images produced after the scratching in which the central areas are those where different applied normal forces were used in attempts to remove the inhibitor molecules by the AFM tip were. The same tip was used in the three experiments shown in Figure 7, in order to maintain consistent conditions. When the applied normal force was <2 nN, i.e. less than the critical force for the tip to penetrate the inhibitor film, the image revealed the surface morphology of the adsorbed inhibitor (Figure 7a). When the normal force was set to 40 nN, the tip slightly penetrated the inhibitor film and created features shown in image Figure 7b. However, because the force was insufficient to remove molecules from the surface, the inhibitor film appears to be more or less intact after the scratching procedure. When the applied normal force was set to 60 nN, the inhibitor molecules were removed from the scratched area, as shown in the center of the image in Figure 7c. Further increases in the applied normal force beyond 60 nN did not change the depth of the scratched area while the underlying much harder mica surface was not scratched by the tip. Figure 8 shows the AFM images of the area after scratching, in 0.5 CMC and 2 CMC inhibitor solutions, respectively. Line scans show depths of 2 and 4 nm at 0.5 CMC and 2 CMC respectively which approximately corresponds to one and two TOFA imidazolium chloride molecular lengths. That is, it appears that a mono-molecular layer is formed at 0.5 CMC and a bi-layer at 2 CMC, which is consistent with models proposed in some previous publications.[6,15,41-42] The film thickness measurements of 2 and 4 nm were consistent when scratching was repeated in different areas on the mica surface, indicating that a continuous, uniform, adsorbed film had formed over the surface in both cases. The experiment was repeated many times with the same result. To confirm that the measured film thickness was due to adsorbed surfactant molecules, similar experiments were repeated in pure water in the absence of TOFA imidazolium chloride. The images revealed a uniform featureless surface and no effect of scratching could be detected.

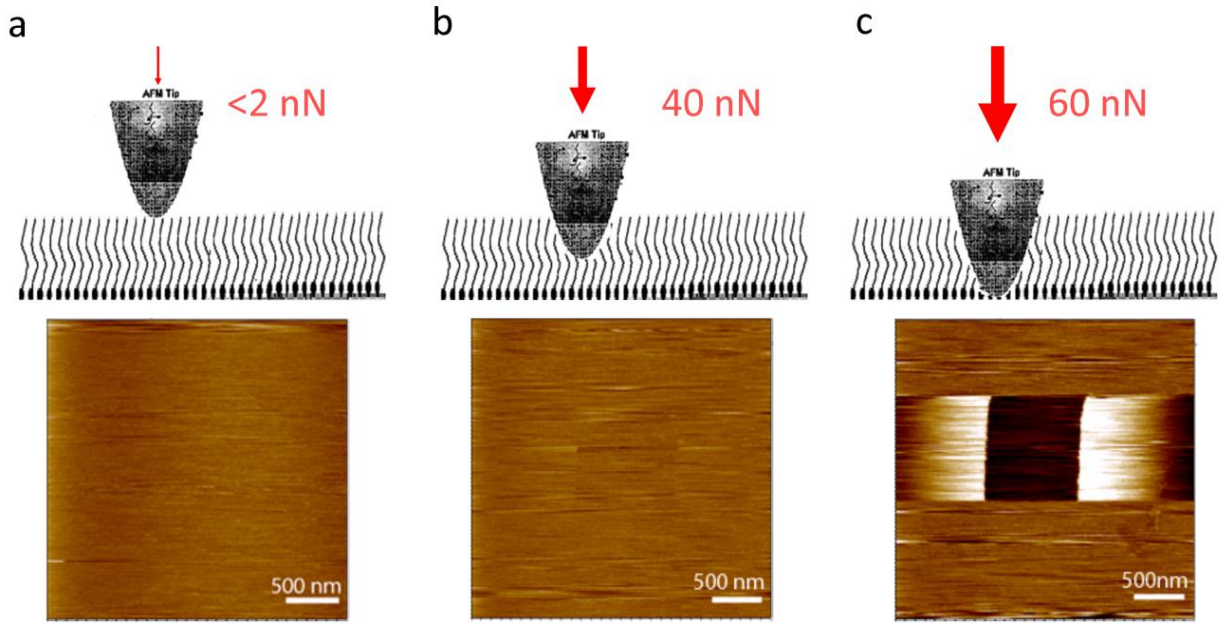

Figure 7: **Topography images of inhibitor films formed at 2 CMC and scanned using different normal forces applied to the cantilever: a) <2 nN, b) 40 nN, c) 60 nN. Each of these images is accompanied with a schematic diagram showing the AFM tip-inhibitor film interaction.**

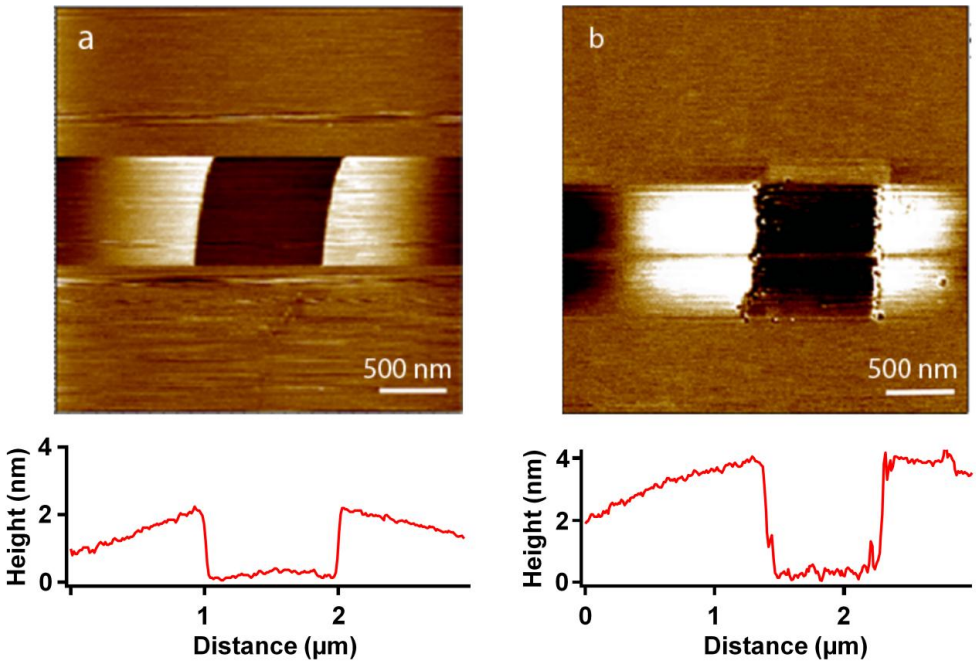

Figure 8. Film thickness measurements for TOFA imidazolium chloride on mica surface at concentrations of (a) 0.5 CMC and (b) 2 CMC. The film thickness was determined by measuring the height difference between scratched and unscratched areas. The 2 nm and 4 nm depths at 0.5 CMC and 2 CMC conditions correspond to the monolayer and bilayer structures, respectively.

Kinetics of re-adsorption

An obvious question emerged following these film thickness measurements was why the inhibitor molecules did not re-adsorb after being scratched from the surface? It was hypothesized that the kinetics of re-adsorption was relatively slow. A new series of experiments was conducted and profile

measurements taken at different time intervals after scratching away the inhibitor molecules in a 2 CMC solution. Figure 9 shows topography images and profiles following the inhibitor layer removal by scratching in the center area described above. The depth of the scratched area was 4 nm at the beginning – immediately following the removal process (Figure 9a), corresponding to the thickness of a bilayer film. The scratched area was gradually "restored" (Figure 9b and c) as the inhibitor re-adsorbed, and it appears fully covered by inhibitor molecules after 6 hours (Figure 9d). These data explain why 6 hours was used to obtain a full layer of adsorbed inhibitor on mica, before any measurements were done, as described in the section above. It also demonstrates the ability of the AFM technique to characterize the kinetics of inhibitor film formation which is important information for any modeling purposes as well as for many practical applications such as: inhibitor batch treatment and in cases where pigging or sand production operations can temporarily destroy the inhibitor film on pipe surfaces.

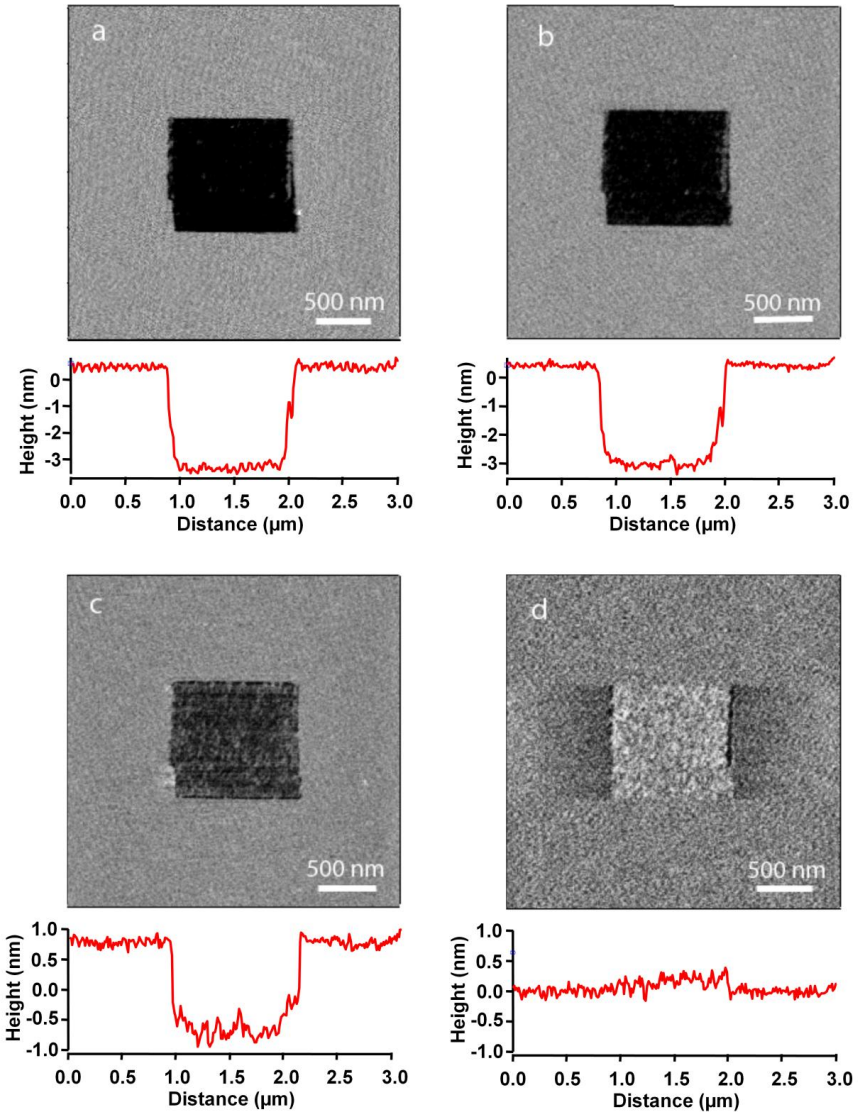

Figure 9: Topography images and surface profiles of an area (a) immediately (b) 1 hr, (c) 3 hr and (d) 6 hr after film removal. The scratched area was gradually restored by inhibitor molecules in 6 hours.

Penetration force measurements

Although it is not fully understood how protective inhibitor films form, the effectiveness of the film to reduce corrosion could be generally related to: molecular size (length), film thickness and packing

density of the adsorbed inhibitor molecules.[43-45] The integrity and persistence of the inhibitor film in flowing solutions is also of paramount importance in pipeline situations. In this section it is described how some mechanical properties of an inhibitor film were evaluated using AFM force-distance measurements. Figure 10 shows force-distance curves measured on inhibitor films formed on mica from aqueous solutions at 0.5 CMC and 2 CMC solutions. These curves are compared to the curve obtained for bare mica, i.e. mica immersed in pure water in the absence of surfactant inhibitor molecules. The Y axis shows the measured force applied to the AFM tip, and the X axis represents the position of tip in the direction perpendicular to the surface.

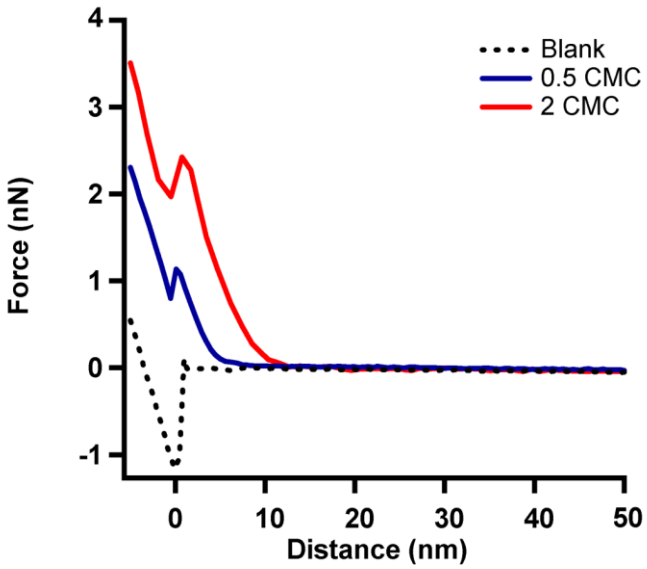

Figure 10: Penetration force measurements on mica surface in the absence and presence of corrosion inhibitor TOFA imidazolium chloride.

On the bare mica surface, which is free of adsorbed surfactant molecules, the force between the tip and surface is zero when the distance is larger than 5 nm, indicating that there is no interaction of the AFM tip with the surface. When the distance of the tip is approximately 5 nm (see black dotted curve), one can observe a "jump to contact" event, i.e. the tip is suddenly attracted to the surface due to short-range attractive forces, which manifests itself as a negative force in Figure 10. Further downward movement of the AFM tip pushes it against the hard mica surface and the resulting repulsion produces a positive force which increases linearly with distance due to flexing of the cantilever. As mica can be considered to be an incompressible substrate under these experimental conditions, one can use the linear part of the approach curve to extract the normal angular sensitivity of the AFM tip. The distance measured from the contact point where the tip touches the mica surface is not the exact distance the tip has moved as it includes a component due to the bending of the AFM cantilever.

In the presence of surfactant inhibitor films, the tip is initially far from the surface and therefore does not interact with it, as illustrated by the zero force measured on the initial part of the curve to the left. As the tip moves downwards approaching the surface, it starts interacting with the outer portion the inhibitor film only at a given distance. This interaction is revealed by an increasing positive/repulsive force. It is thought that this force results in an indentation (or compression) of the inhibitor film produced by the AFM tip. This repulsive force reaches a maximum here called "breakthrough" force corresponding to a situation where the tip starts penetrating the inhibitor film. This situation is followed by an abrupt decrease in repulsive force, corresponding to further incursion of the tip inside the film. Further movement of the AFM tip towards the surface causes the force to increase again as the tip is presses against the mica surface, as already observed in the absence of inhibitor film. In the case of the films formed at 0.5 CMC and 2 CMC, the breakthrough force is measured at about 1.1 nN and 2.4 nN respectively. One can also notice that the force required to penetrate the thicker film resulting from a 2 CMC inhibitor concentration is appreciably higher.

Other authors have used this force-curve technique to determine the thickness of adsorbed molecules, however, while it may provide an indication of film thickness within an order of magnitude (~ 10 nm in our results), it is not considered to be accurate enough. The technique described above of film nano-scratching followed by a line profile measurement gives a more accurate measurement of film thickness. The force-distance measurements when used to determine film thickness usually lead to an overestimation of the film thickness. This is because part of the measurement involves sensing the interaction between the AFM tip and adsorbed inhibitor molecules due to van der Waal type forces which are sensed further away from the inhibitor surface.

However, the force-distance measurements described above provide valuable information about the force required to penetrate an inhibitor film. The force exerted by the flow of fluid in pipelines is usually expressed in terms of a wall shear stress (force/unit area) with units of Pascal (Pa). In order to roughly compare the AFM penetration force measurements with the forces produced by fluid flow, the AFM measurements were converted into a pressure form (Pa) by dividing by the penetration force with the cross-sectional area (πr^2) of the hemispherical shaped apex of the AFM tip. The radius of curvature, of ~15 nm, was obtained from the high resolution image of the AFM tip shown in Figure 3b. Using this radius a cross-sectional area of 7×10^{-16} m^2 is calculated. The measured penetration forces of 1.1 and 2.4 nN can be converted to shear stress of 1.6 and 3.4 MPa respectively for inhibitor films formed at 0.5 CMC and 2 CMC (Table 1).

Table 1. Summary of AFM measurements for inhibitor films on mica, Au and X65 steel substrates.

Substrate and inhibitor concentration		Surface morphology	Film thickness (nm)	Normal film penetration		Lateral film removal (Adhesive Force)	
				Force (nN)	Stress (MPa)	Force (nN)	Stress (MPa)
Mica Air	0.5 CMC	Flat film	2	1.1	1.6	40	57
	2 CMC	Flat film	4	2.4	3.4	44	63
Au Air	2 CMC	Flat film	~5	0.9	1.3	35	50
X65 Steel N_2	0.5 CMC	Flat film	2	1.6	2.3	75	107
	2 CMC	Flat film	4	3.1	4.4	75	107

A mechanism for inhibitor failure in flowing solutions has been repeatedly attributed to the wall shear stress removing inhibitor films from steel pipe walls[31-34]. The typical values of shear stress in pipe flow are in the range of 1 -10 Pa, with 1 kPa fluctuations seen under the most extreme conditions in multiphase slug flow.[46-48] Based on our penetration force measurements, it appears that an MPa level stress is required to break through the inhibitor film. Therefore, from this coarse order-of-magnitude type of comparison, it seems unlikely that realistic fluid flow can physically damage the adsorbed inhibitor film.

However, this comparison can be considered unfair as it involves a force required to penetrate inhibitor films measured perpendicular to the sample surface, whereas the wall shear stress is a result of shearing forces parallel to the surface. In other words, the penetration force is probably related to the mutual interactions between the adsorbed inhibitor molecules and not to the force between the inhibitor molecules and the substrate surface. Furthermore, these measurements were made on mica and not on steel. In order to address these concerns, lateral force measurements were carried out first on mica and then progressed to gold and X65 grade mild steel. The results and discussion of these measurements are given in subsequent sections of this paper.

Interestingly, the penetration of the inhibitor film by the AFM tip did not damage the film structure or observably remove any inhibitor molecules. Figure 11 shows repeated, uninterrupted, force-distance penetration curves recorded at the same position on the mica surface. After 15 repeated penetrations, the film appeared still intact as indicated by the similar force/distance curves and mechanical resistance to the AFM tip. This suggests that the penetration only temporarily/elastically "pushed apart" the inhibitor molecules and when the tip was withdrawn they returned to their original positions with their overall structure intact. AFM images of the area where the penetration measurements were carried out also did not show any defects or damage of the film due to tip penetration. Results suggest that inhibitor molecules remained adsorbed on the surface even when the film was penetrated.

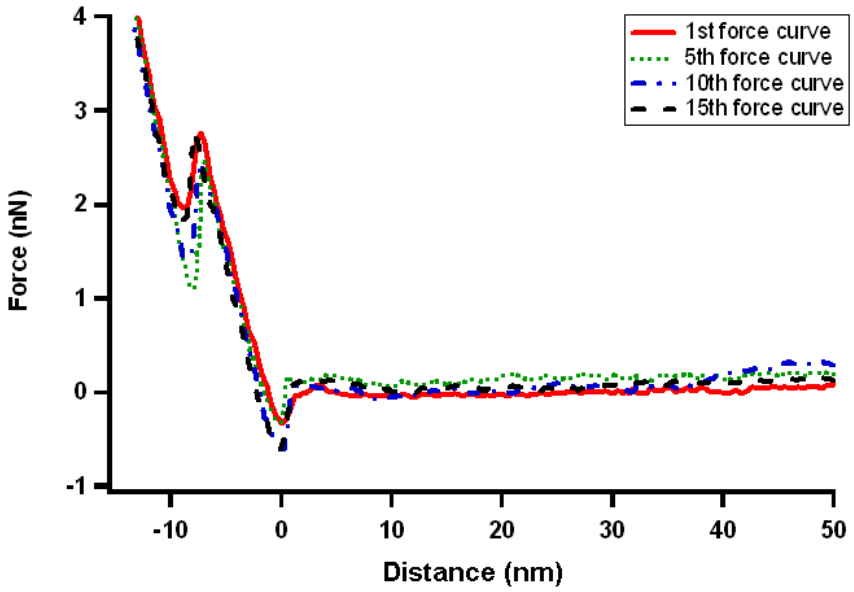

Figure 11: Repeated penetration force measurements at the same position on mica surface in a 2 CMC solution of TOFA imidazolium chloride.

Lateral removal force measurements

While the inhibitor molecules were not removed by AFM tip penetration, removal of inhibitor molecules was achieved by scratching seen during the film thickness tests as described above, due to the lateral interaction between the tip and the adsorbed molecules. In this section, it is reported how AFM was used to quantitatively measure the magnitude of the lateral force required to remove adsorbed inhibitor molecules from the surface. These types of force measurements more closely relate to the adhesive force acting between the inhibitor molecule and the substrate surface.

The lateral force was measured by applying the minimum required high normal force of 60 nN to the cantilever, as described above for the film thickness measurements. At this force, it was found that the inhibitor molecules could be removed from the surface by the scanning tip (see Figure 7 and Figure 8). It was moreover established that this normal force is far larger than the breakthrough force (1.1 or 2.4 nN). To perform a lateral force measurement, a "cyclic line scan", also called a "friction loop", was used. The AFM tip was initially brought into contact with the substrate surface at a 60 nN normal force and then it was moved in one direction, (trace), and then traversed back to the starting point by scanning in the reverse direction (re-trace). Both trace and re-trace were dome in the direction perpendicular to the length of the cantilever and they were using the same scan speed. A "positive" lateral flexing of the cantilever in the forward scan and a "negative" lateral flexing in the reverse scan ensured that the forward and reverse traces did not fully overlap. The AFM instrument records the cantilever torque

induced by the lateral interaction between the AFM tip and the sample surface. The lateral spring constant and AFM photodiode lateral sensitivity were used to convert the raw data into quantitative force values.

Figure 12 and Figure 13 show lateral force measurements for a mono-molecular layer and a bi-molecular layer film formed at 0.5 CMC and 2 CMC solutions respectively. In each of these figures, there are two sets of friction loops recorded on two different surfaces, one for a mica surface in water (blank) and the other is for a mica surface covered with an inhibitor film in an aqueous solution of the inhibitor at the corresponding concentration. The curves were recorded using the same tip, scan speed and normal force (60 nN) applied to the cantilever. Positive and negative friction forces shown in the graphs correspond to the force recorded during the forward and reverse scan respectively. The friction loops shown in Figure 12 and Figure 13 are an average of five force magnitude measurements, recorded during the forward and reverse scans. In Figure 12, the average lateral force on inhibitor free mica was 163 nN while the average lateral force in the presence of the monolayer inhibitor film (0.5 CMC) was 203 nN. The significant increase in the lateral force of 40 nN is attributed to a change in surface properties and the force to remove adsorbed inhibitor molecules from the mica surface.
In Figure 13, the magnitude of the lateral force measurements recorded on a bi-layer inhibitor film in a solution at 2 CMC are very similar to those obtained with a monolayer film in Figure 12. The average lateral force on inhibitor free mica was 163 nN while the average lateral force in the presence of the monolayer film was 207 nN. These results provide evidence that these lateral force measurements are related to the adhesive force acting between the hydrophilic moiety of the molecules in the first molecular-layer and the mica surface.

The lateral or adhesive force measurements were converted into a shear stress by using the same cross-sectional area of 7 x 10^{-16} m^2 as in the penetration force measurements (Table 1). It is difficult to know the exact contact area during friction experiments, i.e. the actual area of the tip acting on the inhibitor molecules during lateral movement. Therefore, the values of shear stress in Table 1 (MPa) are estimated values, but nevertheless suitable for order-of-magnitude comparisons to the wall shear stress produced by fluid flow in pipelines. Table 1 shows the measured lateral forces and calculated stress values. The calculated shear stress to remove the monolayer and bilayer inhibitor films are of the order of 60 MPa, which is at least four-orders of magnitude larger than the wall shear stress encountered in realistic flow in pipelines under the most severe hydrodynamic conditions. Even considering the possible error in the estimation of contact area, the measured adhesion stress is still orders of magnitude higher than the wall shear stress in a pipe flow. Therefore, it appears unlikely that inhibitor films can be removed from the internal pipe wall by the force of fluid flow alone.

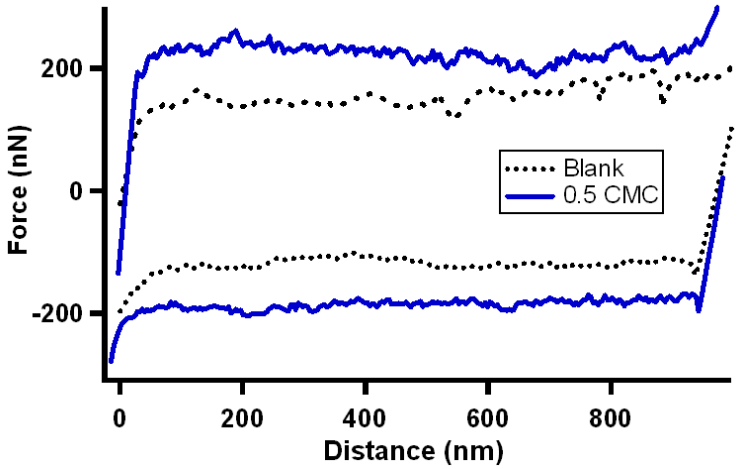

Figure 12: Lateral force measurements on mica surface in the absence and presence of a 0.5 CMC solution of TOFA imidazolium chloride.

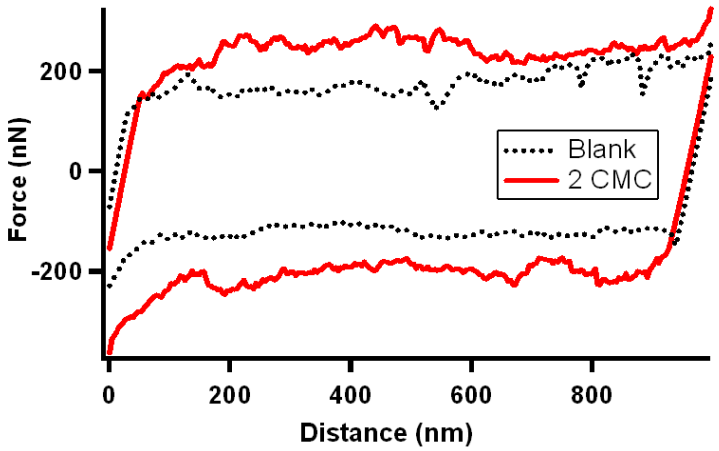

Figure 13: Lateral force measurements on mica surface in the absence and presence of a 2 CMC solution of TOFA imidazolium chloride.

Table 1 provides a summary of normal and lateral force measurements for monolayer and bi-molecular layer films formed on mica from solutions of TOFA imidazolium chloride at 0.5 and 2 times the CMC. It is emphasized again that in Table 1, the force measurements given in nN, which were obtain by AFM force-distance curves and friction loops, are accurate values, directly-determined by AFM force measurements. The numbers for shear stress, in MPa, are calculated values based on the measured forces and the estimated cross-section area of the AFM tip. It can be seen that the lateral force is independent of film thickness and inhibitor concentration, indicating this force is only related to the adhesion between inhibitor hydrophilic groups and mica surface. For a given inhibitor molecule, its adhesion strength on the surface does not change when there are more adsorbed molecules nearby. And the measured lateral force is at least 20 times greater than the corresponding penetration force, indicating it is much harder to physically remove adsorbed molecules than to penetrate through the film structures. In other words, the inhibitor-surface force interactions are much stronger than the inhibitor-inhibitor interactions.

Measurements on gold

To investigate whether the penetration and adhesive forces measured on mica are typical of other surfaces, similar experiments and measurements to those reported above were performed on gold and steel substrates. The measurements for steel are given in the next section. Studies on gold were carried out first because this metal is non-corrosive. Investigations of inhibitor film formation on several substrates helps answer questions such as; is the morphology of the inhibitor films similar and does the normal penetration and lateral adhesive forces exhibited by the film change with a change of substrate. If the mechanical and adhesive properties of inhibitor films on other substrates are similar to mica, it would be additional evidence that inhibitor films cannot be removed from steel surfaces in different corrosive environments, by the forces of fluid flow alone.

AFM images of a vapor deposited gold surface in the absence and presence of TOFA imidazoline at 2 CMC are given in Figure 14. It can be seen from this figure that the gold surface is relatively rough with a peak to peak roughness of 20 nm and the presence of the inhibitor did not change or significantly affect surface roughness. The corresponding penetration force measurements for these surfaces are given in Figure 15. Despite the apparent lack of influence on surface morphology the inhibitor has had an obvious effect on the force distance curve. With no inhibitor present a negative attractive curve was recorded, but in the presence of inhibitor at 2 CMC a positive repulsive force is obtained. The force to

penetrate the inhibitor film is about 2 nN, which is similar to the result for a bi-molecular layer film formed on mica.

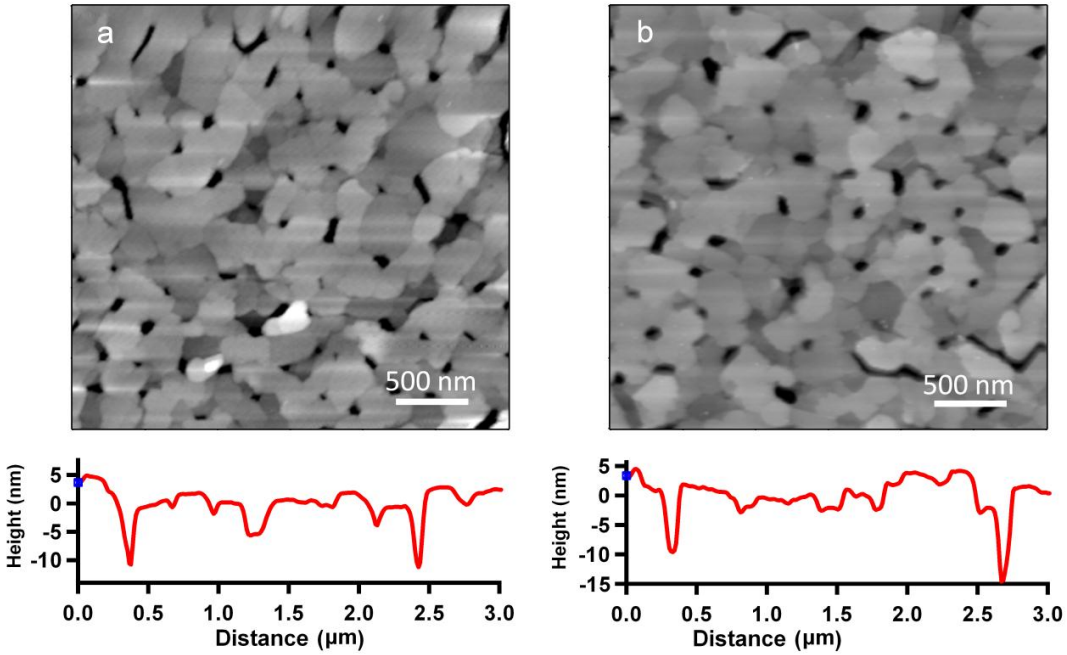

Figure 14: AFM topography images and surface profiles on Au surface in (a) deionized water and (b) a 2 CMC solution of TOFA imidazolium chloride.

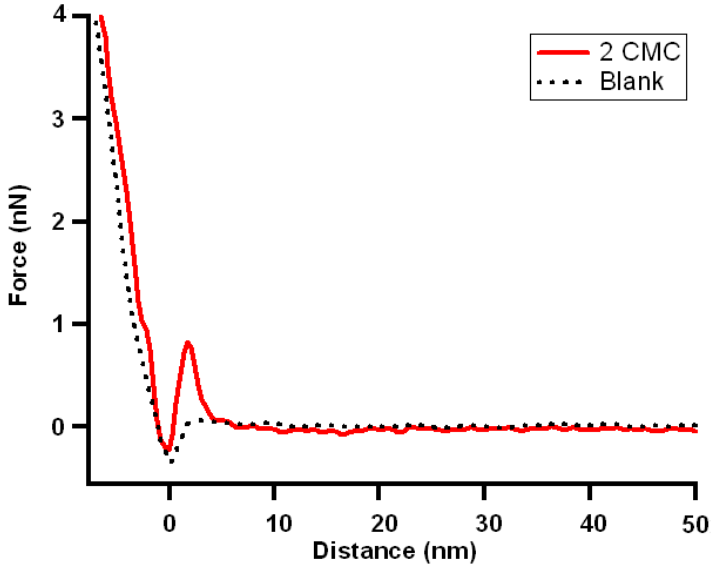

Figure 15: Penetration force measurement on Au surface in the absence and presence of corrosion inhibitor TOFA imidazolium chloride.

Lateral removal force measurements were conducted, firstly, to estimate the thickness of the film and secondly to estimate the force of adhesion. These measurements were performed using a normal load of 60 nN, the same as the load used for mica. An AFM image of the film thickness and surface profile is shown in Figure 16. Figure 17 shows the lateral force measurements for gold in water and in the presence of 2 CMC, TOFA imidazolium chloride. Despite the surface roughness causing some interference with the film thickness measurement, the results are comparable to those recorded for mica (Table 1).

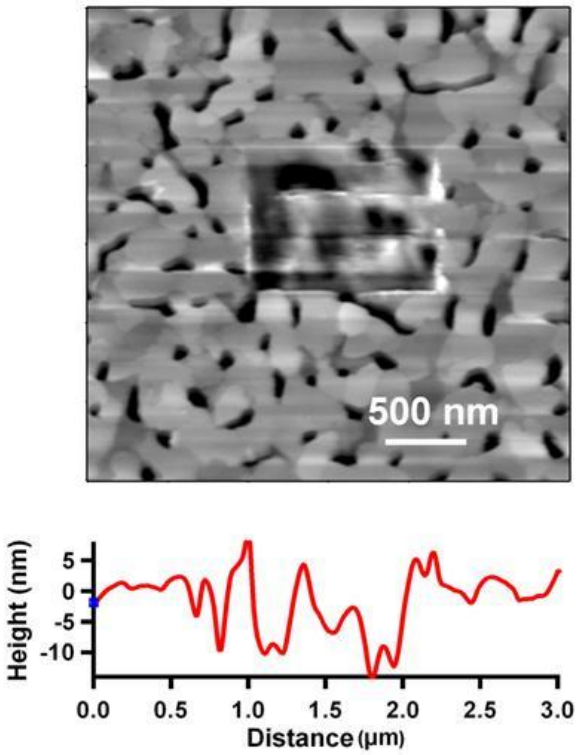

Figure 16: Film thickness measurement of on Au surface in a 2 CMC solution of TOFA imidazolium chloride.

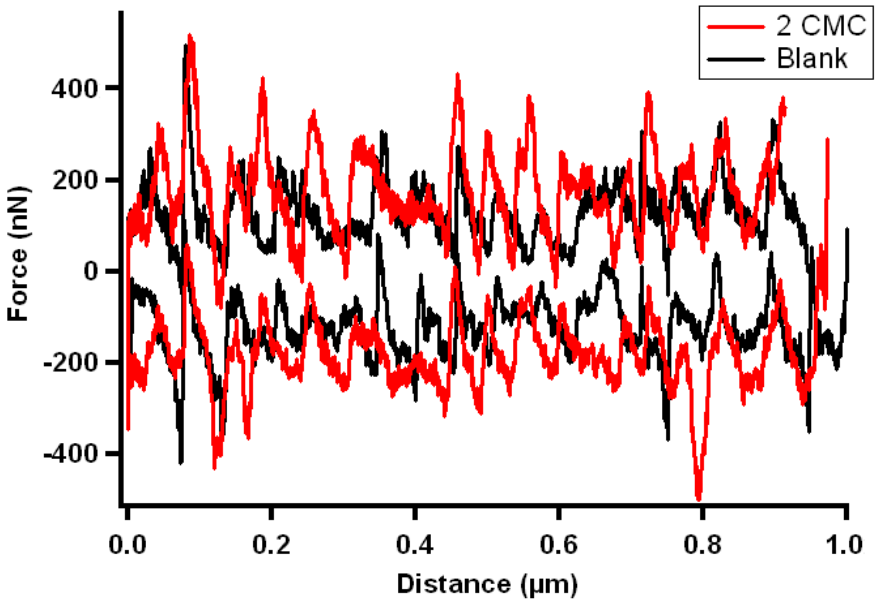

Figure 17: Lateral force measurements on Au surface in a 2 CMC solution of TOFA imidazolium chloride.

Measurements on X65 steel

The work described above using an atomically smooth mica surface and a rough gold surface naturally progressed to carrying out similar measurements on a steel substrate. Imaging of surfactant molecules

adsorbed on steel by AFM has been reported earlier by Bozenberg *et al*.[49] In that investigation, the structure of inhibitor molecules adsorbed on steel were similar to those imaged on mica, but no attempt was made to measure film thickness or the mechanical and adhesive properties of the film.

Adsorption structure and film thickness

Figure 18 shows the topography images and surface profiles of highly polished X65 grade steel in deionized water and aqueous solutions of TOFA imidazolium chloride at concentrations of 0.5 CMC and 2 CMC. These images were obtained from three different locations on the X65 surface and thus the orientations of polishing marks are different. After the polishing, the roughness of steel surface is less than 10 nm (Figure 18a), which makes it eligible for AFM analysis. Further adsorption of inhibitor films (Figure 18b, c) did not change the surface roughness and surface features. This indicates that the adsorption of inhibitor molecules follows the original morphology of the steel surface, and continuous flat films were formed at both 0.5 CMC and 2 CMC conditions.

Film thickness was measured for inhibitor films using the previous described procedure. Figure 19 shows that the film thickness is 2 nm and 4 nm for films formed at 0.5 CMC and 2 CMC respectively, corresponding to the monolayer and bi-molecular layer film formation at respective inhibitor concentrations. These results are consistent with those obtained on mica substrates, indicating this type of inhibitor has similar adsorption properties on mica and steel surface.

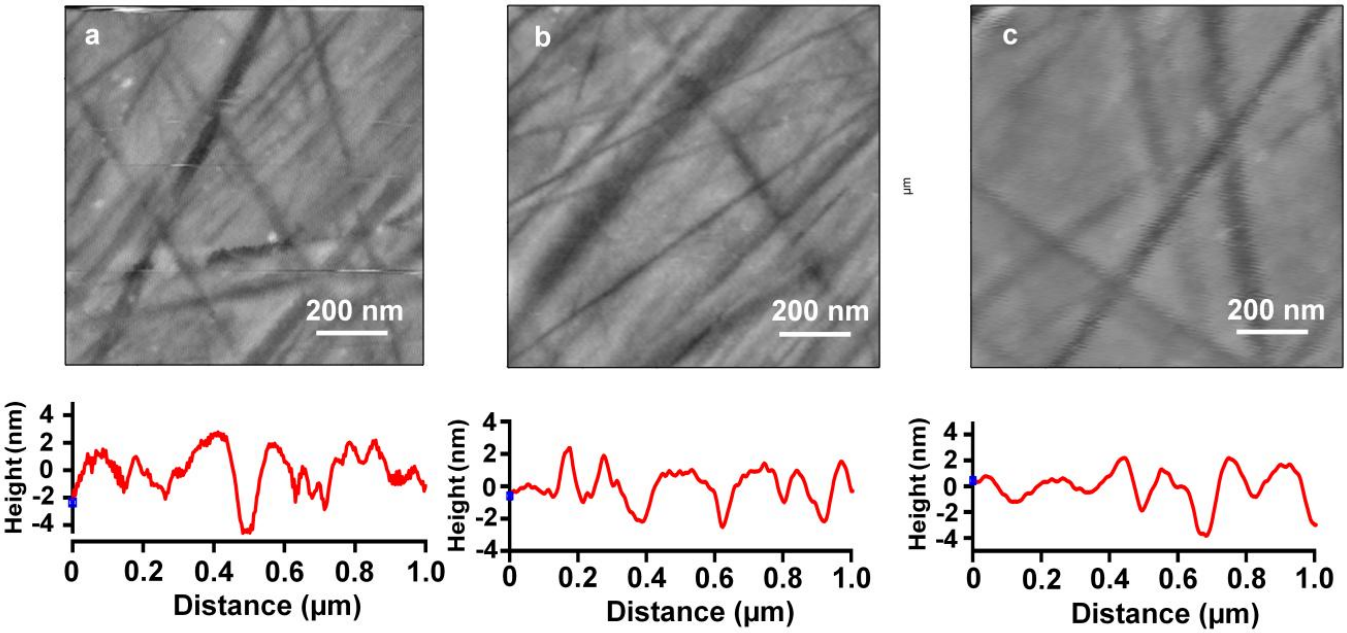

Figure 18: AFM topography images and surface profiles of polished X65 steel surface in (a) deionized water, (b) 0.5 CMC and (c) 2 CMC solutions of TOFA imidazolium chloride.

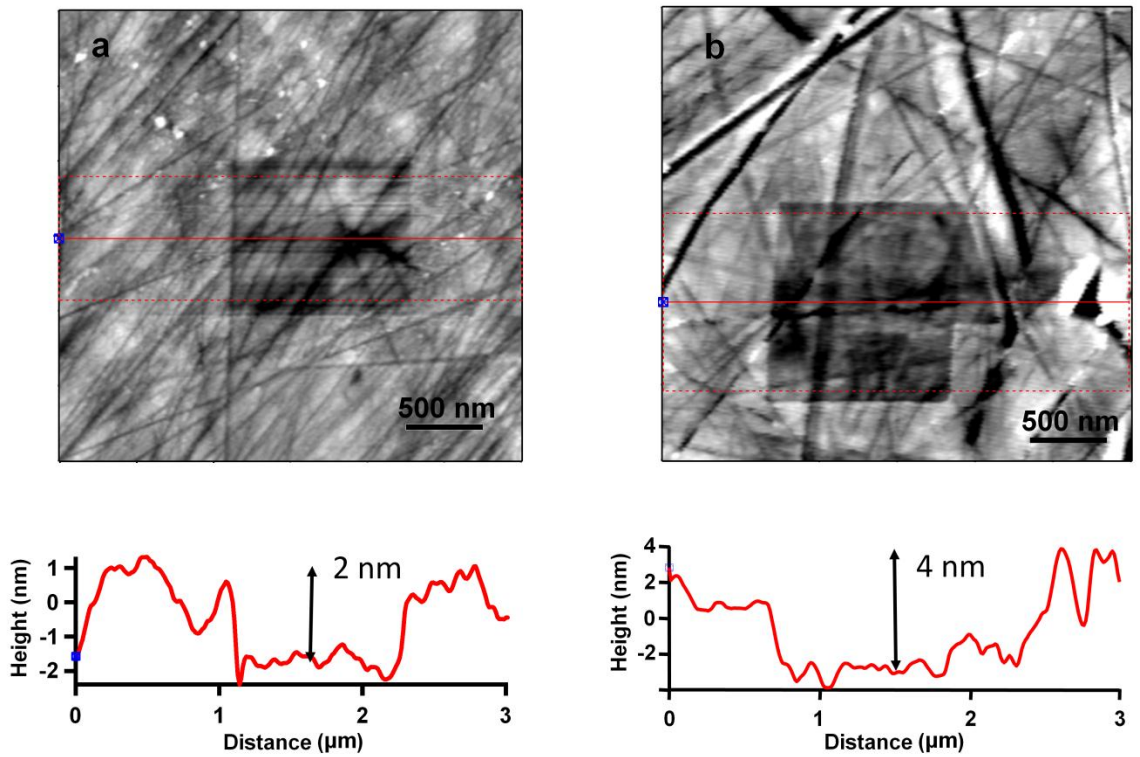

Figure 19: Film thickness measurements for TOFA imidazolium chloride on X65 steel surface at concentrations of (a) 0.5 CMC and (b) 2 CMC.

Penetration force measurements

Figure 20 shows force distance curves, using X65 grade steel as the substrate, in deionized water and the presence of inhibitor films formed at 0.5 CMC and 2 CMC. The force to penetrate the inhibitor films are given in Table 1. Table 1 also provides a summary of the penetration force and lateral removal force measurements recorded at different inhibitor film thicknesses for mica, gold and X65 grade steel. It can be seen that the shape of the curves using X65 grade steel as a substrate are similar to those obtained using a mica substrate. The presence of an inhibitor film has significantly changed the shape of the force-distance curves compared to the blank. The force to penetrate the bi-molecular layer film, formed at 2 CMC, is about 3 nN and is twice the force to penetrate the mono-molecular layer film formed at 0.5 CMC. These results are also consistent with the forces recorded on the mica substrate.

Lateral removal force measurements

Figure 21 shows the friction loop curves for monolayer and bi-molecular layer films of TOFA imidazolium chloride on X65 steel in solutions at 0.5 CMC and 2 CMC. These curves are compared to the friction loop curve for X65 steel in deionized water with no inhibitor present. The technique was the same as that used for mica with a normal load of 60 nN applied to the cantilever. The lateral removal force or adhesive force for the surfactant molecules was determined from the difference in the two curves, i.e. by subtracting the average force in the presence of an inhibitor film from the average force obtained with no inhibitor film present. The molecular adhesive force was determined to be about 75 nN for both the mono and bi-molecular layer films. As anticipated, the results are independent of film thickness since they are a measurement of the adhesive force between the molecules hydrophilic head group and the substrate surface. By further converting these lateral force values to stress values, based on the cross-section area of the AFM tip, the stress to physically remove inhibitor molecules is as high as 100 MPa. Even considering the possible variations in the tip area during the scanning, an MPa level stress value is required to remove inhibitor film away from steel surface. These results

indicate that the fluid flow, which only provides a shear stress less than 1000 Pa, can cause the removal of inhibitor in a pipeline.

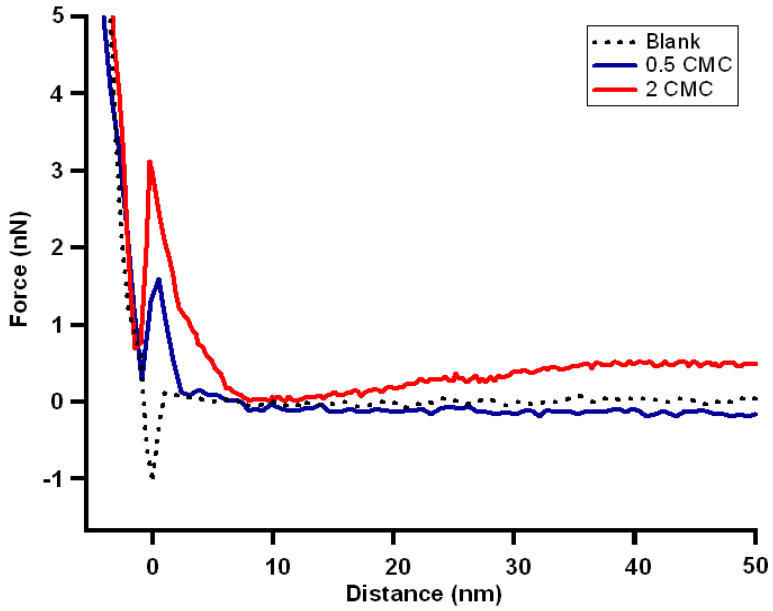

Figure 20: Penetration force measurements on X65 steel surface in the absence and presence of TOFA imidazolium chloride.

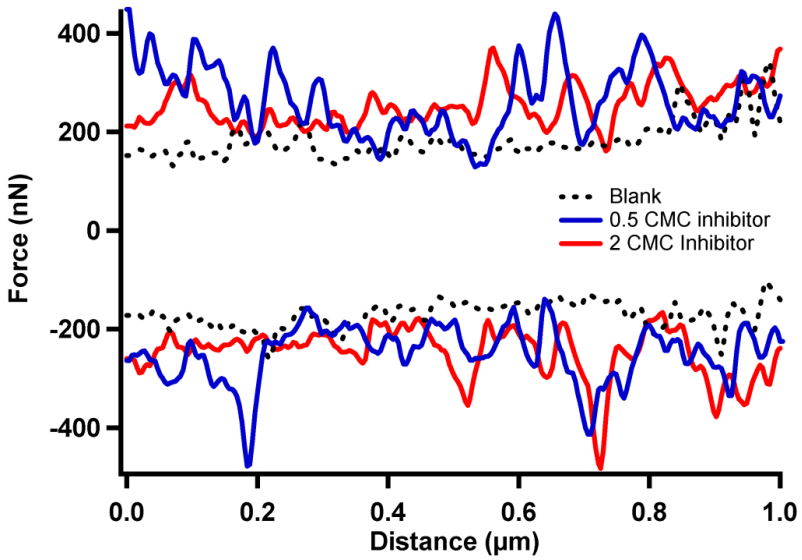

Figure 21: Lateral force measurements on X65 steel surface in the absence and presence of TOFA imidazolium chloride.

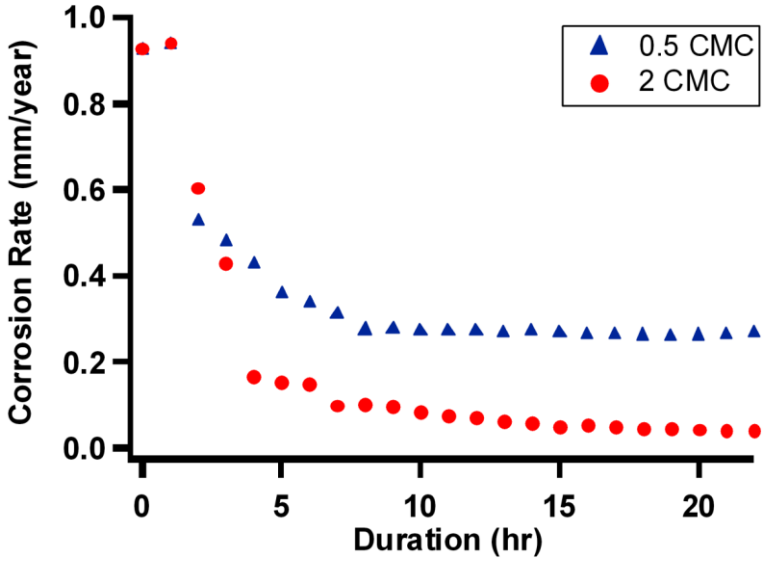

Figure 22: Corrosion rates were measured on X65 steel specimens in 0.5 CMC and 2 CMC solutions of TOFA imidazolium chloride. In both conditions, corrosion rate reached a steady state after adding inhibitors for 5 to 6 hours.

Corrosion rate measurements

In order to connect inhibitor performance to the AFM measurements, particularly those for X65 grade steel, corrosion rate measurements were conducted for X65 steel in carbonic acid (CO_2 saturated solution 10 g/L NaCl in deionized water) at TOFA imidazolium chloride concentrations of 0.5 and 2 times the CMC. Figure 22 shows corrosion rate versus time measurements for the two inhibitor concentrations. The corrosion rates were obtained using the linear polarization resistance (LPR) technique. In both cases, the initial corrosion rate was high and reduced to lower rates due to the presence of the inhibitor. It took 5-6 hours to achieve a steady state corrosion rate and maximum level of protection. This time is similar to the time detected by AFM for the inhibitor film to re-adsorb on mica. The higher steady state corrosion rate of 0.26 mm/y obtained at an inhibitor concentration of 0.5 CMC can be attributed to the formation of a less protective mono-molecular layer film. On the other hand, the lower corrosion rate of 0.05 mm/y, at an inhibitor concentration of 2 CMC, can be attributed to the formation of a more protective bi-molecular layer film as proven by the AFM measurements.

CONCLUSIONS

We have found that TOFA imidazolium chloride inhibitor films formed a continuous and uniform film on mica, gold and X65 grade steel surfaces. The measurements indicated that a monolayer formed below the critical micelle concentration (CMC), i.e. at 0.5 CMC, while a bi-layer formed above the CMC, i.e. at 2 CMC.

Force measurement used to penetrate the inhibitor films is related to film structure. A significantly greater force was required to penetrate bi-layer than monolayer films but both were found to be about 20 to 40 times lower than that required to remove the inhibitor films during nano-scratching tests. This indicates corrosive species may diffuse through the protective film structure and reach the metal surface even when the inhibitor film still exists. Lateral removal force measurement is directly related to the strength of adhesion between the molecules hydrophilic group and the substrate surface and not to the number of inhibitor molecular layer, as these measurements were independent of film thickness.

The shear stress required to remove inhibitor molecules from the surface determined by AFM lateral force measurements was found to be 50-100 MPa, which is at least three orders of magnitude above the maximum shear stress obtained by fluid flow in pipelines (<1 kPa) even under the most severe hydrodynamic conditions. Therefore, it is unlikely that this type of inhibitor film can be removed from steel pipe walls due to shear forces produced by fluid flow.

An appreciable error may exist in converting AFM force measurements (Newton) to a shear stress (Pascal), due to the uncertainty of knowing the actual area of the AFM tip interacting with the adsorbed molecules of the inhibitor film. Nevertheless, due to the huge magnitude in difference between the AFM determined shear stress and the hydrodynamic wall-shear stresses obtained in practice, the above conclusion is considered valid.

ACKNOWLEDGMENTS

Dr C. Deslouis is warmly acknowledged for fruitful discussions. The International Relations Office of Univ. P. & M. Curie (Paris, France) is warmly acknowledged for the financial support of the collaboration between LISE and ICMT (Ohio University, USA).

REFERENCES

1 Y. Duda, R. Govea-Rueda, M. Galicia, H.I. Beltran, L.S. Zamudio-Rivera, Corrosion inhibitors: Design, performance, and computer simulations, J Phys Chem B. 109 (2005) 22674-22684.

2 E. Garcia-Ochoa, J. Cruz, R. Martinez, J. Genesca, Experimental and theoretical study of 1-(2-ethylamino)-2-methylimidazoline as an inhibitor of carbon steel corrosion in acid media, J Electroanal Chem. 566 (2004) 111-121.

3 M. Du, F.G. Liu, J. Zhang, M. Qiu, Electrochemical behavior of Q235 steel in saltwater saturated with carbon dioxide based on new imidazoline derivative inhibitor, Corros Sci. 51 (2009) 102-109.

4 Z. Jun, J.X. Liu, W.Z. Yu, S.Q. Hu, Y. Long, G.M. Qiao, Molecular modeling study on inhibition performance of imidazolines for mild steel in CO(2) corrosion, Appl Surf Sci. 256 (2010) 4729-4733.

5 M.J. Rosen. *Surfactants and interfacial phenomena*. 3rd edn, (Wiley-Interscience, 2004).

6 S. Paria, K.C. Khilar, A review on experimental studies of surfactant adsorption at the hydrophilic solid-water interface, Adv Colloid Interfac. 110 (2004) 75-95.

7 R. Bordes, J. Tropsch, K. Holmberg, Role of an Amide Bond for Self-Assembly of Surfactants, Langmuir. 26 (2010) 3077-3083.

8 A. Sivakumar, P. Somasundaran, S. Thach, Micellization and Mixed Micellization of Alkylxylenesulfonates - a Calorimetric Study, Colloid Surface A. 70 (1993) 69-76.

9 A. Sivakumar, P. Somasundaran, S. Thach, Calorimetric Investigations on the Effect of Position of Functional-Groups on Surfactant Adsorption, J Colloid Interf Sci. 159 (1993) 481-485.

10 A. Sivakumar, P. Somasundaran, Adsorption of Alkylxylenesulfonates on Alumina - a Fluorescence Probe Study, Langmuir. 10 (1994) 131-134.

11 A.X. Fan, P. Somasundaran, N.J. Turro, Adsorption of alkyltrimethylammonium bromides on negatively charged alumina, Langmuir. 13 (1997) 506-510.

12 R.K. Thomas, D.C. Mcdermott, G. Fragneto, Neutron Reflection from Surfactants and Polymers Adsorbed at the Solid-Liquid Interface, Abstr Pap Am Chem S. 210 (1995) 193-COLL.

13 G. Fragneto, J.R. Lu, D.C. McDermott, R.K. Thomas, A.R. Rennie, P.D. Gallagher, S.K. Satija, Structure of monolayers of tetraethylene glycol monododecyl ether adsorbed on self-assembled monolayers on silicon: A neutron reflectivity study, Langmuir. 12 (1996) 477-486.

14 S. Manne, J.P. Cleveland, H.E. Gaub, G.D. Stucky, P.K. Hansma, Direct Visualization of Surfactant Hemimicelles by Force Microscopy of the Electrical Double-Layer, Langmuir. 10 (1994) 4409-4413.
15 R. Atkin, V.S.J. Craig, E.J. Wanless, S. Biggs, Mechanism of cationic surfactant adsorption at the solid-aqueous interface, Adv Colloid Interfac. 103 (2003) 219-304.
16 X.H. Li, G.N. Mu, Tween-40 as corrosion inhibitor for cold rolled steel in sulphuric acid: Weight loss study, electrochemical characterization, and AFM, Appl Surf Sci. 252 (2005) 1254-1265.
17 P.M. Karlsson, M.W. Anderson, A.E.C. Palmqvist, Adsorption of sodium dodecyl sulfate and sodium dodecyl phosphate at the surface of aluminium oxide studied with AFM, Corros Sci. 52 (2010) 1103-1105.
18 A. Imanishi, M. Suzuki, Y. Nakato, In situ AFM studies on self-assembled monolayers of adsorbed surfactant molecules on well-defined H-terminated Si(111) surfaces in aqueous solutions, Langmuir. 23 (2007) 12966-12972.
19 X.H. Cui, S.Z. Mao, M.L. Liu, H.Z. Yuan, Y.R. Du, Mechanism of surfactant micelle formation, Langmuir. 24 (2008) 10771-10775.
20 C. Gutig, B.P. Grady, A. Striolo, Experimental studies on the adsorption of two surfactants on solid-aqueous interfaces: Adsorption isotherms and kinetics (vol 24, pg 4806, 2008), Langmuir. 24 (2008) 13814-13814.
21 C. Bellmann, A. Synytska, A. Caspari, A. Drechsler, K. Grundke, Electrokinetic investigation of surfactant adsorption, J Colloid Interf Sci. 309 (2007) 225-230.
22 N.R. Chevalier, C. Chevallard, P. Guenoun, Monovalent Cations Trigger Inverted Bilayer Formation of Surfactant Films, Langmuir. 26 (2010) 15824-15829.
23 S. Manne, H.E. Gaub, Molecular-Organization of Surfactants at Solid-Liquid Interfaces, Science. 270 (1995) 1480-1482.
24 J.F. Liu, G. Min, W.A. Ducker, AFM study of adsorption of cationic surfactants and cationic polyelectrolytes at the silica-water interface, Langmuir. 17 (2001) 4895-4903.
25 C.E. Jhuma Das, Susan Perkin, and Max L. Berkowitz*, Restructuring of Hydrophobic Surfaces Created by Surfactant Adsorption to Mica Surfaces, Langmuir. 27 (2011) 5.
26 R.D. Tilton, S.B. Velegol, B.D. Fleming, S. Biggs, E.J. Wanless, Counterion effects on hexadecyltrimethylammonium surfactant adsorption and self-assembly on silica, Langmuir. 16 (2000) 2548-2556.
27 J.B. Valim, P.C. Pavan, E.L. Crepaldi, G.D. Gomes, Adsorption of sodium dodecylsulfate on a hydrotalcite-like compound. Effect of temperature, pH and ionic strength, Colloid Surface A. 154 (1999) 399-410.
28 X.H. Li, S.D. Deng, G.N. Mu, H. Fu, F.Z. Yang, Inhibition effect of nonionic surfactant on the corrosion of cold rolled steel in hydrochloric acid, Corros Sci. 50 (2008) 420-430.
29 P. Somasundaran, Q. Zhou, Synergistic adsorption of mixtures of cationic gemini and nonionic sugar-based surfactant on silica, J Colloid Interf Sci. 331 (2009) 288-294.
30 L.C.d.M. Tania Farías, Jerzy Zajac, Aramis River, Benzalkonium chloride and sulfamethoxazole adsorption onto natural clinoptilolite: Effect of time, ionic strength, pH and temperature, J Colloid Interf Sci. 363 (2011) 11.
31 G. Schmitt, Drag reduction by corrosion inhibitors - A neglected option for mitigation of flow induced localized corrosion, Mater Corros. 52 (2001) 329-343.
32 Y. Chen, W.P. Jepson, EIS measurement for corrosion monitoring under multiphase flow conditions, Electrochim Acta. 44 (1999) 4453-4464.
33 Y.G. Zheng, X. Jiang, W. Ke, Effect of flow velocity and entrained sand on inhibition performances of two inhibitors for CO2 corrosion of N80 steel in 3% NaCl solution, Corros Sci. 47 (2005) 2636-2658.
34 S.O. Saad Ghareba, The effect of electrolyte flow on the performance of 12-aminododecanoic acid as a carbon steel corrosion inhibitor in CO2-saturated hydrochloric acid, Corros Sci. 53 (2011) 8.
35 E. Gulbrandsen, S. Nesic, A. Stangeland, T. Burchardtt, Effect of Precorrosion on the Performance of Inhibitors for CO2 Corrosion of Carbon Steel; NACE International: Houston, TX, 1998; Corrosion/98, Paper 13.

36 G. Binnig, C.F. Quate, C. Gerber, Atomic Force Microscope, Phys Rev Lett. 56 (1986) 930-933.
37 D.A. Lopez, S.N. Simison, S.R. de Sanchez, Inhibitors performance in CO2 corrosion EIS studies on the interaction between their molecular structure and steel microstructure, Corros Sci. 47 (2005) 735-755.
38 S.W. Xia, M. Qiu, L.M. Yu, F.G. Liu, H.Z. Zhao, Molecular dynamics and density functional theory study on relationship between structure of imidazoline derivatives and inhibition performance, Corros Sci. 50 (2008) 2021-2029.
39 J. Zhang, J.X. Liu, W.Z. Yu, Y.G. Yan, L. You, L.F. Liu, Molecular modeling of the inhibition mechanism of 1-(2-aminoethyl)-2-alkyl-imidazoline, Corros Sci. 52 (2010) 2059-2065.
40 E.S. Chan, B.B. Lee, P. Ravindra, New drop weight analysis for surface tension determination of liquids, Colloid Surface A. 332 (2009) 112-120.
41 B.G. Sharma, S. Basu, M.M. Sharma, Characterization of adsorbed ionic surfactants on a mica substrate, Langmuir. 12 (1996) 6506-6512.
42 S. Boufi, S. Alila, M.N. Belgacem, D. Beneventi, Adsorption of a cationic surfactant onto cellulosic fibers - I. Surface charge effects, Langmuir. 21 (2005) 8106-8113.
43 D. Asefi, M. Arami, A.A. Sarabi, N.M. Mahmoodi, The chain length influence of cationic surfactant and role of nonionic co-surfactants on controlling the corrosion rate of steel in acidic media, Corros Sci. 51 (2009) 1817-1821.
44 Y.G. Zheng, X. Liu, Effect of hydrophilic group on inhibition behaviour of imidazoline for CO(2) corrosion of N80 in 3% NaCl solution, Corros Eng Sci Techn. 43 (2008) 87-92.
45 T.G. Harvey, S.G. Hardin, A.E. Hughes, T.H. Muster, P.A. White, T.A. Markley, P.A. Corrigan, J. Mardel, S.J. Garcia, J.M.C. Mol, A.M. Glenn, The effect of inhibitor structure on the corrosion of AA2024 and AA7075, Corros Sci. 53 (2011) 2184-2190.
46 L.C. Maley, W.P. Jepson, Wall shear stress and differential pressure in large-diameter horizontal multiphase pipelines, J Energ Resour-Asme. 122 (2000) 193-197.
47 C.B. G. Schmitt, M. Muller, G. Siegmund, A Probabilistic Model for Flow Induced Localized Corrosion, Corrosion/2000. Paper No. 49 (2000).
48 G.S. R. Hausler, Hydrodynamic and Flow Effects on Corrosion Inhibition, Corrosion. Paper No. 4402 (2004).
49 D.J. S. Bosenberg, T. Becker, S. Bailey, and R. De Marco Resolving the Structure of Carbon Dioxide Corrosion Inhibitors on Surfaces, Corrosion Control 007, Paper 113. (2007).